blood®
Regular Article

MYELOID NEOPLASIA

FLT3^{ITD} drives context-specific changes in cell identity and variable interferon dependence during AML initiation

Yanan Li,[1,2] Wei Yang,[3] Riddhi M. Patel,[1,2] Emily B. Casey,[1,2] Elisabeth Denby,[1,2] Jonny Mendoza-Castrejon,[1,2] Priscilla Rodriguez-Lopez,[1,2] and Jeffrey A. Magee[1-3]

[1]Division of Hematology and Oncology, [2]Department of Pediatrics, and [3]Department of Genetics, Washington University School of Medicine, St. Louis, MO

KEY POINTS

- ***Flt3^{ITD}*** **activates distinct transcriptional programs via distinct enhancers when it cooperates with *NUP98* and *Runx1* mutations.**
- ***Flt3^{ITD}*** **and NUP98-HOXD13 selectively activate type I interferon signaling and thus create a context-specific pathway dependency.**

Acute myeloid leukemia (AML) initiation requires multiple rate-limiting mutations to cooperatively reprogram progenitor cell identity. For example, *FLT3* internal tandem duplication (*FLT3^{ITD}*) mutations cooperate with a variety of different initiating mutations to reprogram myeloid progenitor fate. These initiating mutations often skew toward either pediatric or adult AML patient populations, though *FLT3^{ITD}* itself occurs at similar frequencies in both age groups. This raises the question of whether *FLT3^{ITD}* might induce distinct transcriptional programs and unmask distinct therapeutic vulnerabilities when paired with pediatric, as opposed to adult AML-initiating mutations. To explore this possibility, we compared AML evolution in mice that carried *Flt3^{ITD}/NUP98-HOXD13* (*NHD13*) or *Flt3^{ITD}/Runx1^{DEL}* mutation pairs, which are respectively most common in pediatric and adult AML. Single-cell analyses and epigenome profiling revealed distinct interactions between *Flt3^{ITD}* and its cooperating mutations. Whereas *Flt3^{ITD}* and *Flt3^{ITD}/Runx1^{DEL}* caused aberrant expansion of myeloid progenitors, *Flt3^{ITD}/NHD13* drove the emergence of a pre-AML population that did not resemble normal hematopoietic progenitors. Differences between *Flt3^{ITD}/Runx1^{DEL}* and *Flt3^{ITD}/NHD13* cooperative target gene expression extended to fully transformed AML as well. *Flt3^{ITD}/NHD13* cooperative target genes were enriched in human *NUP98*-translocated AML. *Flt3^{ITD}/NHD13* selectively hijacked type I interferon signaling to drive expansion of the pre-AML population. Blocking interferon signaling delayed AML initiation and extended survival. Thus, common AML driver mutations, such as *FLT3^{ITD}*, can coopt different mechanisms of transformation in different genetic contexts. Furthermore, pediatric-biased NUP98 fusions convey actionable interferon dependence.

Introduction

FLT3-internal tandem duplication (*FLT3^{ITD}*) is one of the most common mutations found in both pediatric and adult acute myeloid leukemia (AML).[1,2] It typically arises late in AML evolution,[3] and it is insufficient to cause AML by itself.[4] Instead, *Flt3^{ITD}* cooperates with a range of different initiating mutations to drive AML.[5-12] When paired with *Tet2*, *Runx1*, or *Npm1* mutations, *Flt3^{ITD}* induces changes in gene expression and epigenome organization that are not observed with any of these individual mutations alone.[9-11,13] The target gene profiles overlap,[10] suggesting that *Flt3^{ITD}* may activate a core set of AML effectors irrespective of which mutations it cooperates with. However, the prior studies all described interactions between *Flt3^{ITD}* and mutations that occur more commonly in adult AML than in pediatric AML. Approximately, 70% of early childhood AML carry translocations that express fusion oncoproteins, whereas only ~10% of older adult AML are driven by fusion proteins.[1] *FLT3^{ITD}* may therefore convey distinct mutation profile- and age-specific gene dependencies when it pairs with pediatric fusions as opposed to adult initiating mutations.

Cryptic *NUP98* translocations (*NUP98*-t) are AML driver mutations that arise most often in young children and frequently cooccur with *FLT3^{ITD}*.[1,14-16] NUP98 has several fusion partners, including NSD1, KDM5A, HOXA9, and HOXD13.[14] NUP98 fusion proteins create phase-separated condensates at target gene loci to physically approximate enhancer and promoter elements.[17,18] They recruit transcriptional coactivators, including MLL1 and NSL complexes, to *HOX* genes to promote transcript expression.[19-22] *HOX* gene products then reprogram hematopoietic progenitors and drive aberrant self-renewal programs.[19-21] NUP98 fusions require cooperating mutations

to induce AML, with *FLT3*^{ITD} being the most common cooperating mutation (>50%).[1,14,15,22,23] Mouse and human models confirm that *NUP98*-t is not sufficient to initiate AML by itself.[12,22,24,25] *FLT3*^{ITD} interactions with *NUP98*-t therefore offer a prototypical case for comparing pediatric and adult mutation cooperation.

To understand how pediatric and adult initiating mutations might differentially orient *FLT3*^{ITD}-driven transcriptional states, we tested whether *Flt3*^{ITD} has similar or distinct functions in the setting of a pediatric-biased NUP98-HOXD13 (NHD13) mutation as compared to an adult-biased *Runx1* loss-of-function mutation. Through bulk and single-cell sequencing approaches, we found that *Flt3*^{ITD} activated vastly different target genes and different target enhancers when paired with *NHD13* as compared to *Runx1* mutations. *Flt3*^{ITD}*/NHD13* elicited a robust type I interferon (IFN-1) response that was not evident in *Flt3*^{ITD}*/Runx1* mutant progenitors and has not been described for other models of *Flt3*^{ITD} cooperation.[6,7,10,11,13] *Ifnar1* (IFN-1 receptor) deletion depleted *NHD13*-dependent pre-AML cells and reduced expression of genes that have been shown to drive AML self-renewal (eg, *Cdk6* and *Msi2*). This impeded AML initiation and extended survival. Our findings show that *FLT3*^{ITD} coopts different mechanisms of transformation when it pairs with a pediatric-biased NUP98 fusion as compared to adult-biased mutations. Furthermore, the data uncover a therapeutically actionable IFN-1 sensitivity in *NUP98*-translocated AML.

Methods

Mouse lines

All mouse lines are previously published and were obtained from the Jackson Laboratory.[26-29]

Cell analyses and transplantation assays

Cells were isolated, stained, analyzed, and transplanted as previously described.[10,30-35] Western blotting, cell cycle, and annexin V assays were performed as previously described in the study by Porter et al.[10] Expanded descriptions of these previously published methods are available in the supplemental Methods, available on the *Blood* website. Extreme Limiting Dilution Analysis was used to calculate repopulating cell frequencies and to compare genotypes.[36]

CITE-seq library construction, sequencing, and analysis

Bone marrow cells were c-kit selected and stained with tagged Total-Seq B antibodies (BioLegend). We isolated Lineage$^-$c-Kit$^+$ cells (LK) by using flow cytometry and generated libraries with 10× Genomics Chromium Next GEM Single Cell 3′ v3.1, Chromium Single Cell 3′ Feature Barcode Library, Dual Index NT Set A, and Dual Index TT Set A kits according to the manufacturer's instructions. Libraries were sequenced, aligned, and filtered as previously described.[30,37] We performed Iterative Clustering and Guide-gene Selection (ICGS, version 2) with the AltAnalyze toolkit.[38] Gene Set Variation Analysis was performed using a Gaussian kernel.[39] Human RNA-seq data were procured from TARGET,[1] St. Jude Cloud,[40] or The Cancer Genome Atlas.[2]

RNA-seq, ATAC-seq and ChIPmentation

RNA was isolated with RNeasy plus micro kits (Qiagen). Libraries were generated with Clontech SMARTer kits, sequenced on a HiSeq3000 sequencing system, and aligned to mouse Ensembl release 76 top-level assembly using STAR version 2.0.4b.[41] Linear modeling (limma/voom) was used to compare gene expression across samples.[42] False discovery rates (FDRs) were calculated using the Benjamini-Hochberg method. Pathway analysis was performed with Reactome,[43] Generally Applicable Gene-set Enrichment[44] or Gene Set Enrichment Analysis.[45] The IFN-1 target gene set was previously described in the study by Li et al.[30] ATAC-seq and ChIPmentation libraries were generated and analyzed as previously described[30,31,46,47] using established pipelines.[48-50]

Survival studies

Survival of *Vav1-Cre; Flt3*^{ITD}*; NHD13; Ifnar1*$^{+/-}$ and *Vav1-Cre; Flt3*^{ITD}*; NHD13; Ifnar1*$^{-/-}$ mice was compared with the log-rank test. For retrovirus driven leukemias, 500 000 LK cells were isolated from P0 mice, transduced with MSCV-*Flt3*^{ITD}-IRES-mCherry retrovirus, and split among 5 recipients per transduction. Three independent replicates were performed.

Results

Flt3^{ITD} has different effects on MPP expansion and function in the setting of *NHD13* and *Runx1* mutations

We used transgenic and targeted mouse alleles to test whether *Flt3*^{ITD} has distinct effects on hematopoiesis when it cooperates with a pediatric-biased NUP98 fusion protein as compared to an adult-biased *Runx1* deletion. We crossed *Flt3*^{ITD} knock-in mice with *Vav1-NUP98-HOX13* (*NHD13*) transgenic mice to yield *Flt3*^{ITD}*/NHD13* compound mutants.[27,29] We separately generated *Vav1-Cre;Flt3*$^{ITD/+}$*;Runx1*$^{fl/+}$ (*Flt3*^{ITD}*/Runx1*^{DEL}) mice.[10] We quantified hematopoietic stem cells (HSCs; CD150$^+$CD48$^-$ Lineage$^-$Sca1$^+$Kit$^+$) and multipotent progenitors (MPPs; CD48$^+$Lineage$^-$Sca1$^+$Kit$^+$) in compound and single-mutant littermates at postnatal day (P)14. This age was chosen because *NUP98*-t is most frequently associated with early-mid childhood AML. Young adult mice were subsequently analyzed as well. *Flt3*^{ITD}*/NHD13* and *Flt3*^{ITD}*/Runx1*^{DEL} mutation combinations had similar effects on HSCs but dichotomous effects on MPPs. HSCs were severely depleted in both *Flt3*^{ITD}*/NHD13* and *Flt3*^{ITD}*/Runx1*^{DEL} mice at P14 (Figure 1A; supplemental Figure 1). In contrast, *Flt3*^{ITD}*/Runx1*^{DEL} caused a dramatic expansion of the MPP population, whereas *Flt3*^{ITD}*/NHD13* did not (Figure 1B). The FLT3^{ITD} inhibitor, gilteritinib, partially suppressed MPP expansion in *Flt3*^{ITD}*/Runx1*^{DEL} mice after 10 days of treatment (P21-31), whereas it did not significantly reduce MPP numbers in similarly treated *Flt3*^{ITD}*/NHD13* mice (supplemental Figure 2). Similar changes in HSC and MPP numbers were also observed in 8-week-old adult mice (Figure 1C-D), indicating that the impact of these mutations was not restricted to early postnatal stages of ontogeny.

Because HSCs were almost completely depleted in both *Flt3*^{ITD}*/NHD13* and *Flt3*^{ITD}*/Runx1*^{DEL} mice, we tested whether *Flt3*^{ITD}*/NHD13* or *Flt3*^{ITD}*/Runx1*^{DEL} MPPs acquire ectopic repopulating activity that could sustain hematopoiesis. We transplanted 200 sorted MPPs from P14 *Flt3*^{ITD}*/NHD13* or

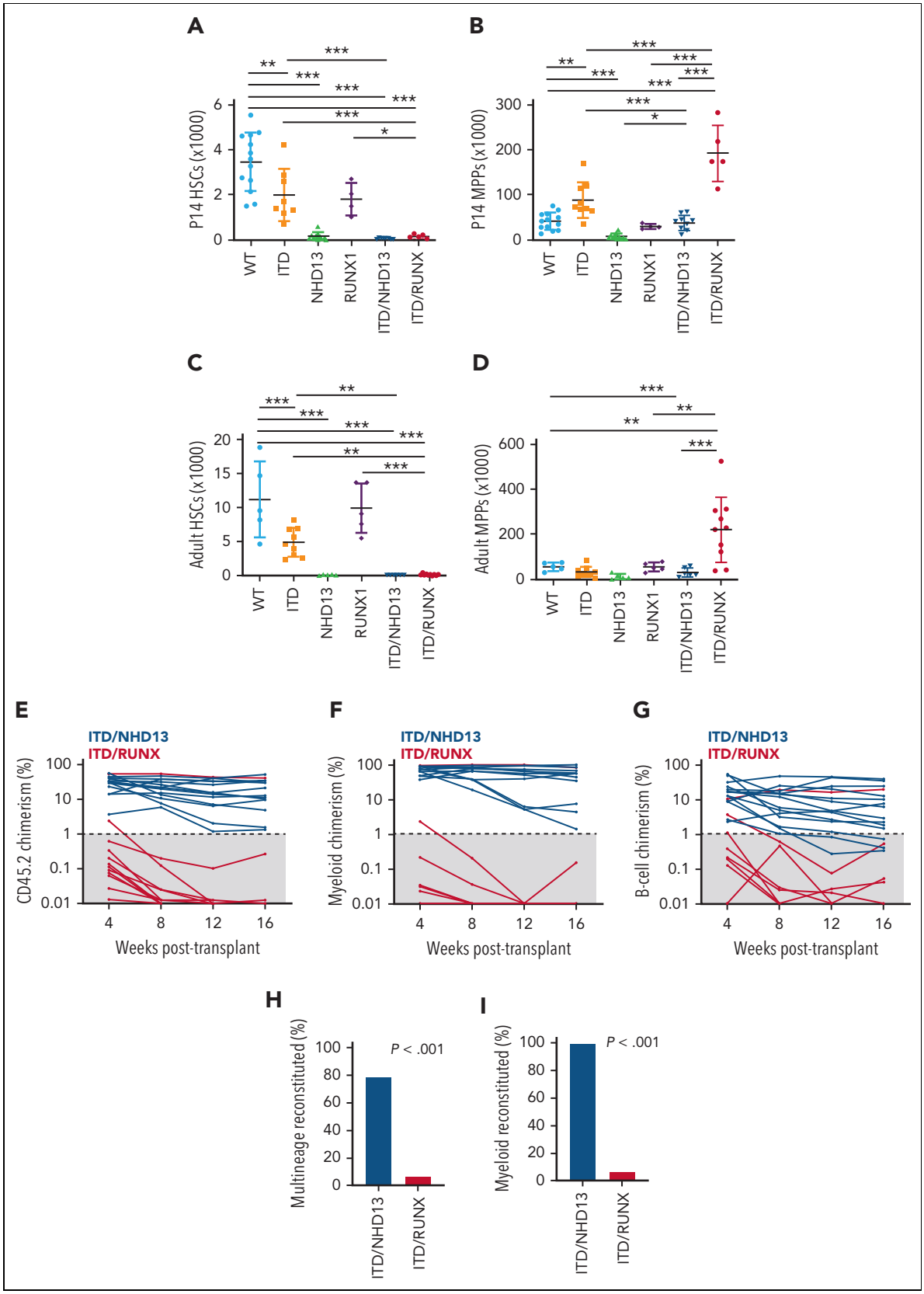

Figure 1. *Flt3*^{ITD}/*Runx1*^{DEL} and *Flt3*^{ITD}/*NHD13* have distinct effects on MPP expansion and repopulating activity. (A-D) HSC and MPP numbers in 2 hindlimbs from P14 or 8-week-old adult mice of the indicated genotypes. n = 4 to 13, **P* < .05, ***P* < .01, ****P* < .001 by one-way ANOVA with Holm-Sidak posthoc test. Error bars reflect the standard deviation. (E-G) Percentage of CD45.2^{+} leukocytes (E), CD11b^{+}Gr1^{+} myeloid cells (F), or B220^{+} B cells (G) in recipient mice after the transplantation of 200 sorted MPPs of the indicated genotypes, along with 300 000 CD45.1 competitor cells. Each line tracks donor chimerism for an individual recipient. n = 13 to 14. (H-I) Percentage of recipients with multilineage (lymphoid + myeloid) or myeloid donor cell chimerism >1%, 16 weeks post-transplant for the indicated donor genotypes. *P* values are shown based on Fisher exact test. ANOVA, analysis of variance.

Flt3^{ITD}/*Runx1*^{DEL} mice, along with 300 000 wild-type CD45.1 competitor bone marrow cells, into lethally irradiated CD45.1 recipient mice. *Flt3*^{ITD}/*NHD13* MPPs were capable of long-term myeloid and lymphoid reconstitution (Figure 1E-I). In contrast, *Flt3*^{ITD}/*Runx1*^{DEL} MPPs failed to repopulate a majority of irradiated recipient mice despite their expanded numbers (Figure 1E-I). Thus, *Flt3*^{ITD}/*NHD13* and *Flt3*^{ITD}/*Runx1*^{DEL} MPPs are functionally distinct, with *NHD13*, but not *Runx1*^{DEL}, conveying ectopic repopulating activity.

Flt3^{ITD}/*NHD13* and *Flt3*^{ITD}/*Runx1* induce distinct patterns of cooperative gene expression and enhancer activation, including an *NHD13*-specific IFN-1 signature

Prior studies have described overlapping cooperative target gene profiles for *Flt3*^{ITD} when it pairs with *Tet2*, *Runx1*, or *Npm1* mutations.[10,11,13] This suggests that *Flt3*^{ITD} might engage a core set of AML effectors, irrespective of which mutations it cooperates with. However, the distinct effects of *Flt3*^{ITD}/*NHD13* and *Flt3*^{ITD}/*Runx1*^{DEL} on MPP function suggest that *Flt3*^{ITD} may engage different effectors when it cooperates with pediatric fusion proteins, such as NHD13. To test this, we performed RNA-seq on P14 *Flt3*^{ITD}/*NHD13* and *Flt3*^{ITD}/*Runx1*^{DEL} MPPs, as well as wild-type and single-mutant littermate controls. We initially focused on P14 to maintain consistency with the phenotypic and functional studies described above. Principal component analysis revealed strikingly different gene expression profiles in *Flt3*^{ITD}/*NHD13* and *Flt3*^{ITD}/*Runx1*^{DEL} MPPs relative to one another and to single-mutant controls (Figure 2A). We identified subsets of genes that were significantly activated in either *Flt3*^{ITD}/*NHD13* or *Flt3*^{ITD}/*Runx1*^{DEL} MPPs relative to wild-type controls (defined as FDR <0.05, fold change ≥2, Figure 2B; supplemental Table 1). We then defined "cooperative target genes" as those that were significantly increased in compound mutant MPPs relative to each respective single mutant population (eg, increased in *Flt3*^{ITD}/*NHD13* vs *Flt3*^{ITD} and *NHD13* alone; FDR <0.05). We observed very little overlap between *Flt3*^{ITD}/*NHD13* and *Flt3*^{ITD}/*Runx1*^{DEL} cooperative target gene sets (Figure 2C). As an alternative approach, we calculated "interaction scores" for each expressed gene as previously described by Liu et al.[51] This scoring system identified genes within *Flt3*^{ITD}/*NHD13* and *Flt3*^{ITD}/*Runx1*^{DEL} MPPs that exhibited greater changes in expression than could be explained through additive effects of each mutation (supplemental Figure 3A). Again, we observed very little overlap between genes that were cooperatively regulated by *Flt3*^{ITD}/*NHD13* and *Flt3*^{ITD}/*Runx1*^{DEL} (supplemental Figure 3B-C; supplemental Table 1).

Next, we tested whether differences between *Flt3*^{ITD}/*NHD13* and *Flt3*^{ITD}/*Runx1*^{DEL} target gene expression were age specific. We previously showed that *Flt3*^{ITD}/*Runx1*^{DEL} has only modest effect on gene expression in P0 MPPs.[10] In contrast, gene set variation analysis (GSVA)[39] showed that *Flt3*^{ITD}/*NHD13* cooperative target genes were already induced by P0 in *Flt3*^{ITD}/*NHD13* mice (supplemental Figure 3D). *Flt3*^{ITD}/*NHD13* and *Flt3*^{ITD}/*Runx1*^{DEL} cooperative target genes were maintained with similar, genotype-specific patterns in 4-week-old MPPs (supplemental Figure 3E-F). Thus, *Flt3*^{ITD} has distinct cooperative interactions with *NHD13* and *Runx1*^{DEL} across multiple ages.

We used ChIPmentation and ATAC-seq to test whether *Flt3*^{ITD} has cooperating mutation-specific effects on the epigenome. To this end, we identified active enhancers (ie, ATAC-seq peaks with overlapping histone H3K4me1 and histone H3K27ac peaks) in *Flt3*^{ITD}/*NHD13* and *Flt3*^{ITD}/*Runx1*^{DEL} MPPs. Among these, 2928 *Flt3*^{ITD}/*NHD13* MPPs, and 1518 enhancers in *Flt3*^{ITD}/*Runx1*^{DEL} MPPs, were hyperactivated relative to wild-type MPPs based on H3K27ac levels that were significantly elevated in the compound mutants with FDR <0.1 (Figure 2D-E; supplemental Table 2). We identified 90 enhancers that were cooperatively activated by *Flt3*^{ITD}/*NHD13* mutations and 244 enhancers that were cooperatively activated by *Flt3*^{ITD}/*Runx1*^{DEL} (ie, significantly greater H3K27ac levels in double mutants compared with every single mutant with FDR <0.1) (Figure 2F-G; supplemental Figure 4A-D). *Flt3*^{ITD}/*NHD13* and *Flt3*^{ITD}/*Runx1*^{DEL} cooperative target enhancers were largely nonoverlapping (Figure 2H). Both enhancer classes were enriched for ETS and RUNX1 binding sites. *Flt3*^{ITD}/*NHD13* target enhancers were also enriched for NKX, GATA, and Zinc-finger family transcription factor binding sites that were not observed in *Flt3*^{ITD}/*Runx1*^{DEL} target enhancers (supplemental Figure 4E). In contrast, *Flt3*^{ITD}/*Runx1*^{DEL} target enhancers were enriched for STAT, TCF, AP-1, and IRF binding sites that were not observed in *Flt3*^{ITD}/*NHD13* target enhancers (supplemental Figure 4F). The latter finding is consistent with data from human AML showing that in adults, FLT3^{ITD} activates AP-1–dependent enhancers via the MAP-kinase pathway.[52] Together, these data show that *Flt3*^{ITD} activates distinct enhancers, via distinct complements of transcription factors, when paired with a pediatric-biased NUP98 fusion as compared to an adult-biased–*Runx1* loss-of-function mutation.

We next sought to identify molecular pathways that might be uniquely activated in *Flt3*^{ITD}/*NHD13* MPPs, given the limited overlap between *Flt3*^{ITD}/*NHD13* and *Flt3*^{ITD}/*Runx1*^{DEL} cooperative target genes. We performed Reactome pathway analysis on cooperative *Flt3*^{ITD}/*NHD13* target genes and found striking enrichment for IFN-1 target genes (Figure 3A). Indeed, almost half of all *Flt3*^{ITD}/*NHD13* cooperative target genes were IFN-1 targets, based on a previously compiled gene set (Figure 3B).[30] IFN-1 target expression was much higher in *Flt3*^{ITD}/*NHD13* MPPs than in any other genotype (Figure 3C). Gene set enrichment analysis confirmed that IFN-1 targets were activated by both *Flt3*^{ITD} and *NHD13* alone, but they were further activated when the mutations cooperated (Figure 3D). Interestingly, *Flt3*^{ITD}/*Runx1*^{DEL} cooperation suppressed the IFN-1 signature relative to *Flt3*^{ITD} alone (Figure 3D). Serum from P14 *Flt3*^{ITD}/*NHD13* contained high levels of IFN-α (Figure 3E) but not IFN-β (data not shown). IFN-1 target gene activation was evident even by P0 in *Flt3*^{ITD}/*NHD13* MPPs (Figure 3F). Thus, *Flt3*^{ITD} cooperates with *NHD13* but not *Runx1*^{DEL} to induce IFNα expression and IFN-1 target genes.

Flt3^{ITD}/*Runx1*^{DEL} and *Flt3*^{ITD}/*NHD13* cooperation yield distinct, emergent progenitor populations

Our functional studies and bulk RNA-seq data raised the question of whether *Flt3*^{ITD} differentially reprograms the differentiation trajectories of hematopoietic progenitors in the setting of *NHD13* and *Runx1*^{DEL} mutations. Since bulk RNA-seq and MPP surface markers might not adequately capture the transcriptional heterogeneity of mutant progenitors, we

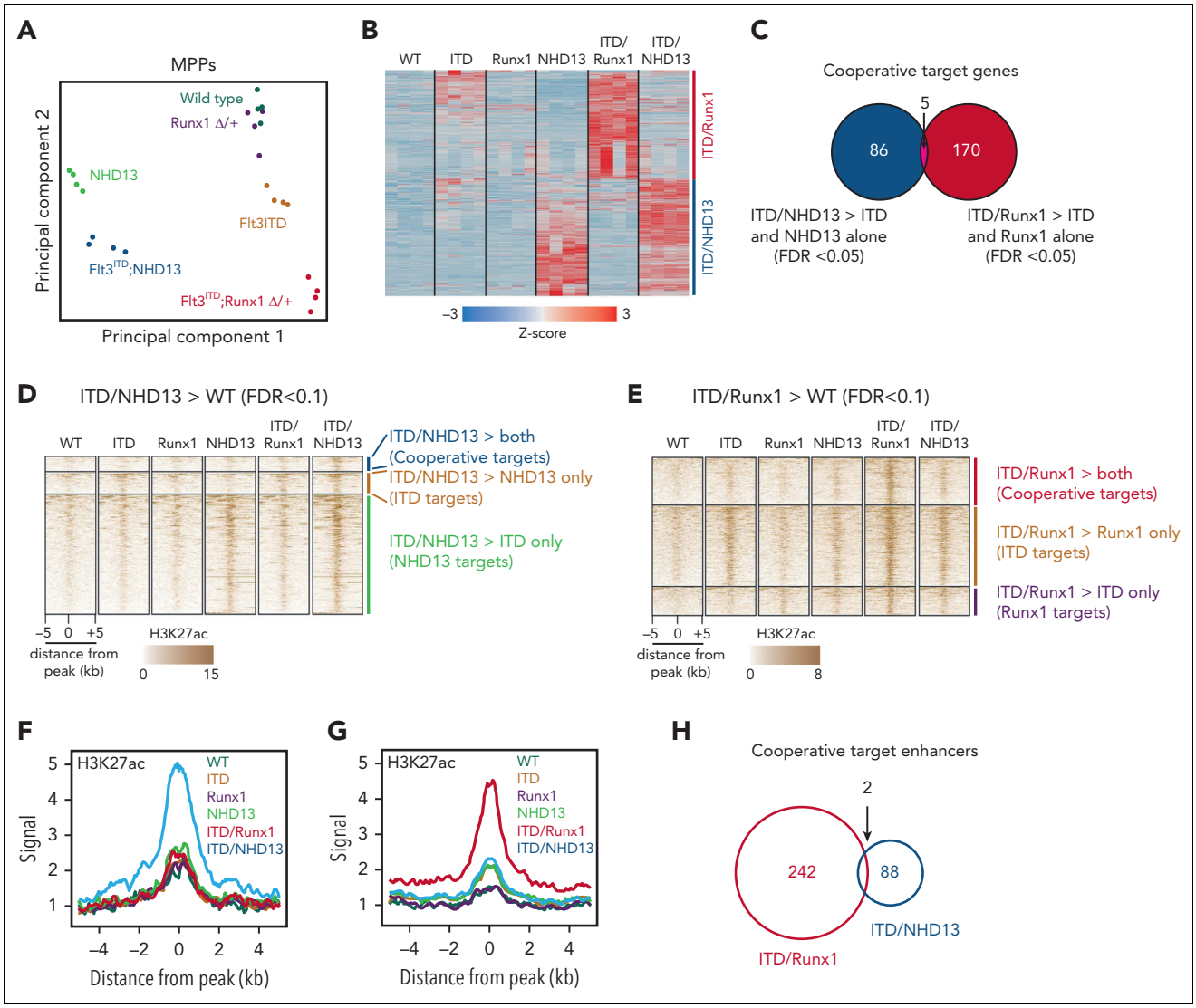

Figure 2. *Flt3*^{ITD}*/Runx1*^{DEL} and *Flt3*^{ITD}*/NHD13* induce distinct cooperative changes in gene expression and enhancer activation. (A) Principal component analysis for MPPs for the indicated genotypes at P14, based on bulk RNA-seq. n = 4 per genotype. (B) Heatmap displaying the expression of genes that were induced in either *Flt3*^{ITD}*/NHD13* or *Flt3*^{ITD}*/Runx1*^{DEL} MPPs, relative to wild-type (FDR < 0.05, positive fold change ≥2). (C) Venn diagram showing minimal overlap between *Flt3*^{ITD}*/NHD13* and *Flt3*^{ITD}*/Runx1*^{DEL} cooperative target genes, defined as genes from panel B with significantly higher expression in compound mutant MPPs relative to both single-mutant MPPs (FDR < 0.05). (D) Heatmap showing H3K27ac levels for enhancers (defined as overlapping ATAC-seq and H3K4me1 peaks) that were more highly active in *Flt3*^{ITD}*/NHD13* MPPs relative to wild-type MPPs, and one or both single mutants (based on H3K27ac peak heights, FDR < 0.1 by DiffBind analysis). Peaks are clustered based on whether H3K27ac levels in the compound mutant are elevated relative to *Flt3*^{ITD} or *NHD13* single mutant MPPs, or both (cooperative target enhancers). (E) A similar heatmap as in panel D, except showing enhancers that were more highly active in *Flt3*^{ITD}*/Runx1*^{DEL} MPPs. (F-G) Aggregate peak heights for cooperative target enhancers from panels D-E, respectively. (H) Venn diagram showing the minimal overlap between *Flt3*^{ITD}*/NHD13* and *Flt3*^{ITD}*/Runx1*^{DEL} cooperative target enhancers.

performed CITE-seq to better delineate how *Flt3*^{ITD}*/NHD13* and *Flt3*^{ITD}*/Runx1*^{DEL} mutations cooperate to reprogram cell identity. We profiled control (×2), *Flt3*^{ITD} (×2), *Runx1*^{DEL}, *Flt3*^{ITD}*/Runx1*^{DEL}, *NHD13*, and *Flt3*^{ITD}*/NHD13* LK cells at P14 (supplemental Table 3). We used Iterative Clustering and Guide Gene Selection, version 2 (ICGS2) to cluster the cells in an unsupervised manner and then overlaid surface marker phenotypes for various progenitor populations based on tagged feature barcodes (Figure 4A; supplemental Figure 5A).[38,53] We observed strong concordance between the replicate control and *Flt3*^{ITD} samples (Figure 4B). Several clusters within the control LK cells aligned with well-defined progenitor populations, based on both surface marker phenotypes and gene expression (Figure 4A-B; supplemental Figure 5B; supplemental Table 4). These included cluster 18 (HSCs/MPPs), cluster 25 (MPP), and clusters 2 and 11 (granulocyte-monocyte progenitors [GMPs]) (supplemental Figure 5B). Control and *Runx1*^{DEL} samples had very similar cluster distributions (Figure 4B), indicating that heterozygous *Runx1*^{DEL} has a very limited effect on hematopoiesis, consistent with the bulk RNA-seq data.

Next, we compared the cluster distributions of *Flt3*^{ITD}, *Flt3*^{ITD}*/NHD13*, and *Flt3*^{ITD}*/Runx1*^{DEL} progenitors to determine whether each genotype confers unique cell identities, and the degree to which mutant progenitors resemble normal progenitors. By itself, *Flt3*^{ITD} caused the expansion of a GMP-like cluster (#11) that was also evident in wild-type mice, and it

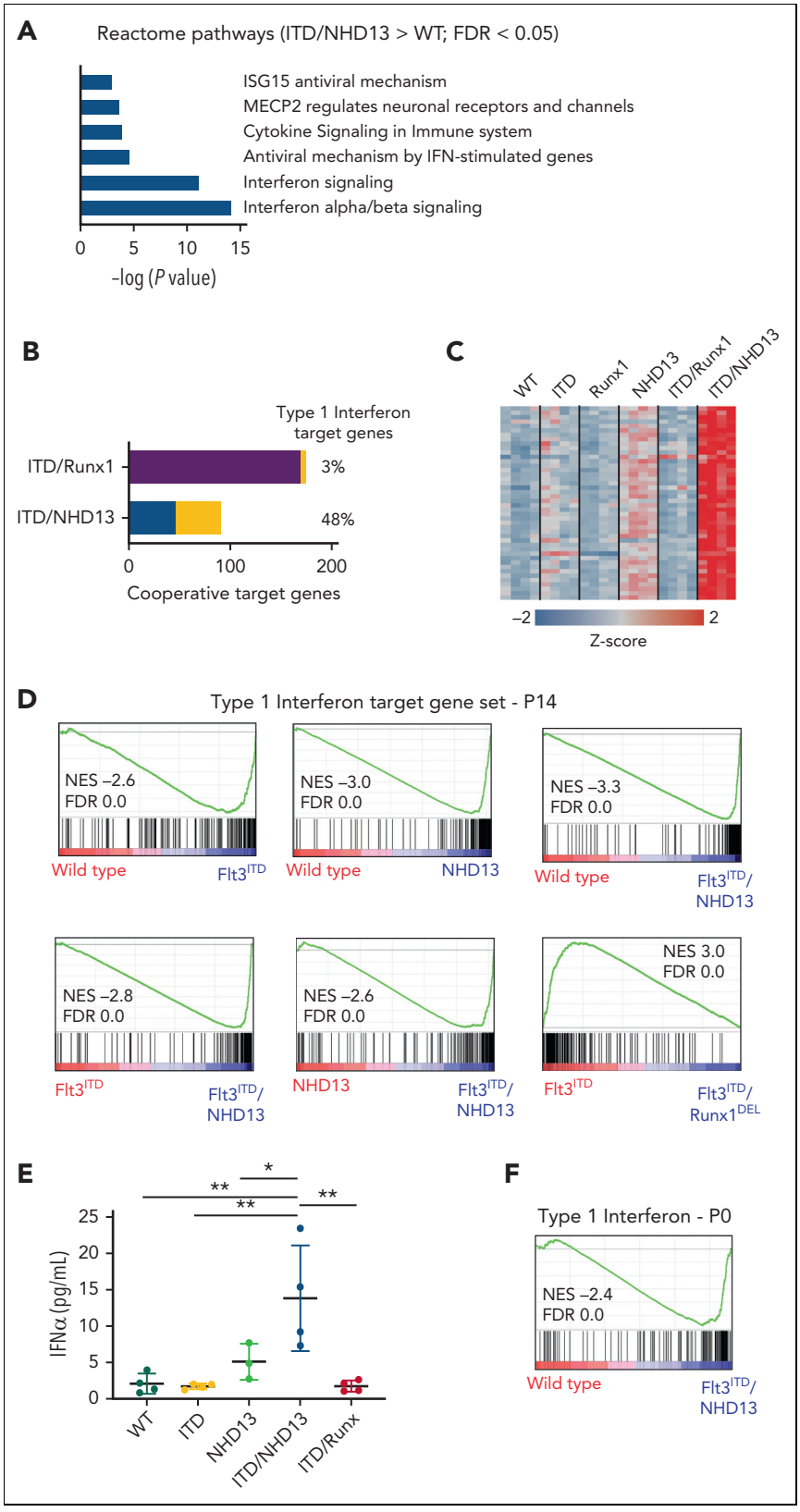

Figure 3. *Flt3*^{ITD}*/NHD13* cooperation results in IFN-1 target gene hyperactivation, in contrast to *Flt3*^{ITD}*/Runx1*^{DEL} cooperation. (A) Reactome pathway analysis of *Flt3*^{ITD}*/NHD13* target genes. (B) Almost half of all genes induced in *Flt3*^{ITD}*/NHD13* MPPs were IFN-1 targets, based on a previous comparison of wild-type and *Ifnar1*$^{-/-}$ MPPs.[30] Only ~3% of genes induced in *Flt3*^{ITD}*/Runx1*^{DEL} MPPs were IFN-1 targets. (C) Heatmap showing expression of IFN-1 targets from panel B in MPPs with the indicated genotypes. (D) Gene set enrichment analysis showing enrichment of IFN-1 targets in *Flt3*^{ITD}*/NHD13* and *Flt3*^{ITD}*/Runx1*^{DEL} MPPs relative to indicated wild-type and single-mutant MPPs. Both *Flt3*^{ITD} and *NHD13* alone activated IFN-1 targets (top row), but the effects were greatly amplified in *Flt3*^{ITD}*/NHD13* MPPs (bottom row). In contrast, the IFN-1 signature was repressed in *Flt3*^{ITD}*/Runx1*^{DEL} MPPs relative to *Flt3*^{ITD} alone. (E) IFNα levels in the serum of P14 mice of the indicated genotypes, as measured by ELISA. n = 3 to 4. Error bars reflect the standard deviation. *P < .05, **P < .01, ***P < .001 by one-way ANOVA with Holm-Sidak posthoc test. (F) GSEA showing activation of IFN-1 targets in *Flt3*^{ITD}*/NHD13* MPPs at P0. ANOVA, analysis of variance; ELISA, enzyme-linked immunosorbent assay; GSEA, gene set enrichment analysis.

led to the emergence of MPP-like clusters (#7 and #10) that were not present in wild-type mice (Figure 4A-C). Concomitant *Flt3*^{ITD}*/Runx1*^{DEL} mutations markedly expanded clusters 10 and 11 at the expense of other normal populations without causing any additional clusters to emerge (Figure 4B-C; supplemental Figure 5C-D). Thus, *Runx1*^{DEL} largely amplifies *Flt3*^{ITD}-dependent changes in hematopoiesis rather than conveying new emergent transcriptional states.

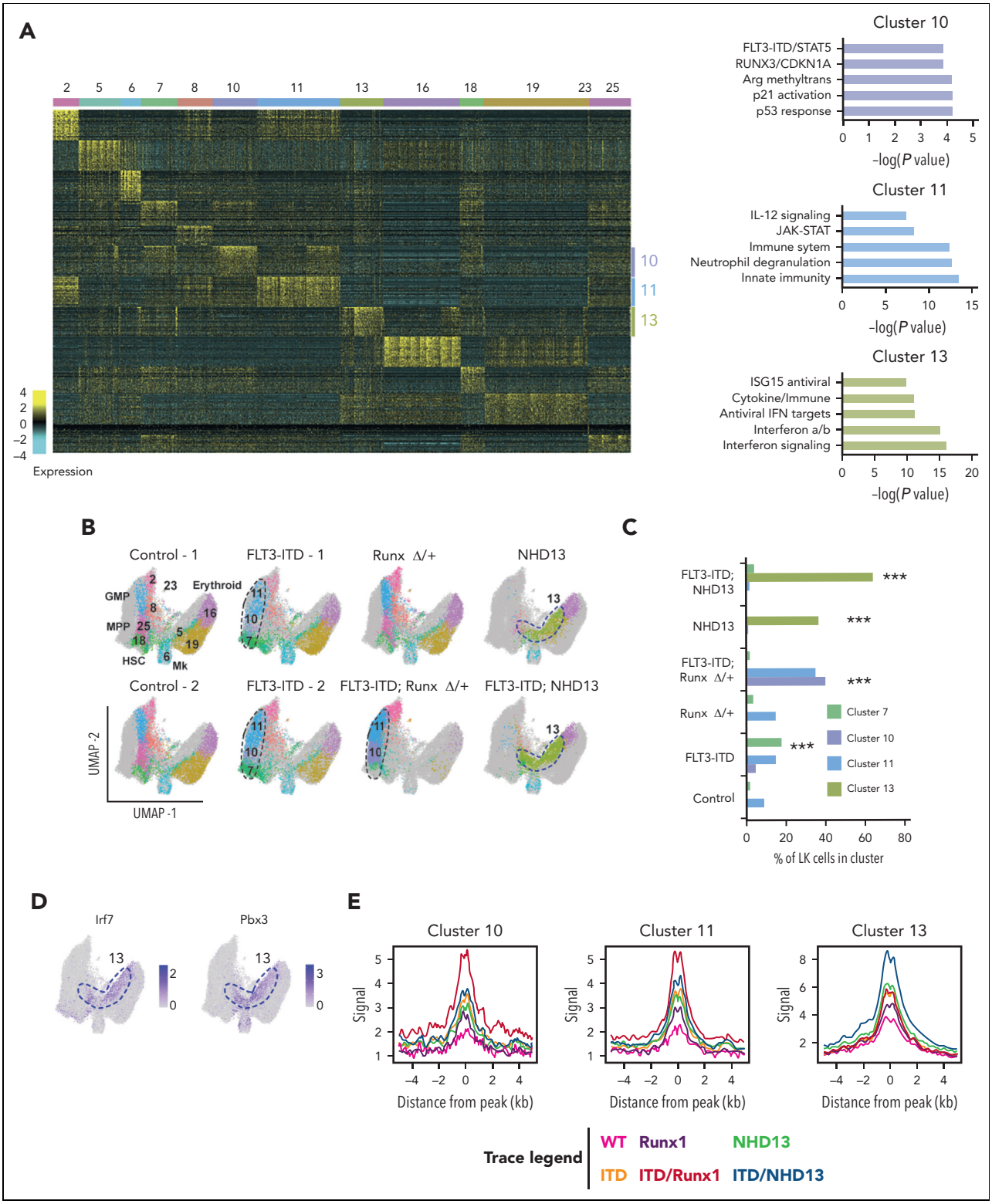

Figure 4. *Flt3*^{ITD}*/NHD13* and *Flt3*^{ITD}*/Runx1*^{DEL} differentially reprogram hematopoietic progenitors. (A) Heatmap showing clustering of single cells and marker genes based on ICGS2. Clusters are designated by colors in the top bar and numbers assigned by the ICGS2 algorithm. Reactome pathway analyses for marker genes for clusters 10, 11, and 13 are shown to the right. (B) Uniform Manifold Approximation and Projection (UMAP) plots demonstrating clusters of cells from ICGS2 for the indicated genotypes. The gray background indicates cells not included in the indicated genotype. Cluster colors are identical to the coloring scheme in panel A. (C) Bar graph showing percentages of cells for each genotype that populate clusters 7, 10, 11, and 13. ***$P < .0001$ by χ^2 test relative to wild-type. The cluster 13 population size was also significantly larger in *Flt3*^{ITD}*/NHD13* relative to single mutants ($P < .0001$). Cluster 10 and 11 sizes were significantly larger in *Flt3*^{ITD}*/Runx1*^{DEL} relative to single mutants ($P < .0001$). (D) Expression of *Irf7*, a canonical IFN-1 target, and *Pbx3*, a canonical NHD13 target, projected onto the UMAP plot. The expression was largely restricted to cluster 13 cells. (E) H3K27ac traces for enhancers that map within 100 kb of marker genes for clusters 10, 11, and 13. ICGS2, Iterative Clustering and Guide Gene Selection version 2.

The *Flt3*^{ITD}/*NHD13* interaction had markedly different effects on cell identity compared with *Flt3*^{ITD}/*Runx1*^{DEL}. *NHD13* caused a cluster (#13) to emerge that was not present in either wild-type or *Flt3*^{ITD} mice (Figure 4A-C). This cluster contained cells with MPP surface marker phenotypes despite clear transcriptional differences between it and normal MPPs (supplemental Figure 5C-D). *Flt3*^{ITD}/*NHD13* cooperation expanded the emergent *NHD13*-specific population, but it did not cause any additional populations to form, nor did it cause the *Flt3*^{ITD}-specific cluster 10 to emerge (Figure 4B-C). We used marker genes affiliated with clusters 10 and 11 (*Flt3*^{ITD}/*Runx1*^{DEL}) and cluster 13 (*NHD13* and *Flt3*^{ITD}/*NHD13*) to test whether the cooperating mutations activate different transcriptional programs and enhancer elements. Reactome pathway analysis showed enrichment of known FLT3^{ITD}/STAT5 target genes, as well as p21 and p53 response genes, in the *Flt3*^{ITD}- and *Flt3*^{ITD}/*Runx1*^{DEL}-specific cluster 10 (Figure 4A; supplemental Table 4). In contrast, it showed enrichment of IFN-1 target genes, such as *Irf7*, in the *NHD13*- and *Flt3*^{ITD}/*NHD13*-specific cluster 13, in addition to canonical NUP98-fusion protein targets, such as *Pbx3* (Figure 4A,D; supplemental Table 4). Enhancers that mapped within 100 kb of cluster 10 and 11 marker genes showed elevated H3K27ac in *Flt3*^{ITD}/*Runx*^{DEL} mice relative to all other genotypes, whereas enhancers that mapped near cluster 13 genes had elevated H3K27ac in *Flt3*^{ITD}/*NHD13* mice (Figure 4E; supplemental Figure 6). These data again show that *Flt3*^{ITD} has profoundly different effects on gene expression, enhancer activation, and cell identity when it cooperates with *NHD13* as compared to *Runx1*^{DEL} mutations. Furthermore, they implicate cells within cluster 13 as putative cells of origin for *Flt3*^{ITD}/*NHD13*-developed AML.

Enhanced *Flt3*^{ITD} expression transforms a unique, isolatable population of *Flt3*^{ITD}/*NHD13* progenitors

To our surprise, *Flt3*^{ITD}/*NHD13* mice did not develop rapid, fully-penetrant AML, in contrast to a prior study.[12] This complicated our efforts to test whether the emergent CITE-seq population (cluster 13) contained bona fide pre-AML cells. The *Flt3*^{ITD} allele used in this study (*Flt3*^{tm1Dgg})[27] differs from the allele used previously to generate AML (*Flt3*$^{tm1.1Dosm}$)[12] in that it retains a floxed PGK-neo cassette in intron 15 that could dampen *Flt3*^{ITD} expression (Figure 5A). We therefore deleted the PGK-neo cassette with *Vav1*-Cre. Mice with the resulting "*Flt3*^{ITDΔ}" allele had elevated STAT5 and extracellular signal-regulated kinase (ERK) phosphorylation in MPPs, relative to wild-type and *Flt3*^{ITD} mice (Figure 5B). Furthermore, *Flt3*^{ITDΔ}/*NHD13* mice now developed rapid, fully penetrant AML within 4 to 6 weeks after birth (Figure 5C). AML cells ectopically expressed B220 (CD45R), consistent with the *Flt3*$^{tm1.1Dosm}$ model (Figure 5D).[12]

To test whether the CITE-seq-defined, *NHD13*-specific population (Figure 4B, cluster 13) was enriched for pre-AML cells, we sought surface markers that would enable isolation by flow cytometry. CD317 (*Bst2*) expression was significantly elevated in *Flt3*^{ITD}/*NHD13* cluster 13 cells, relative to *NHD13* cells and all other clusters (Figure 5E). CD317 could therefore potentially enrich for pre-AML cells. We isolated CD317^{+}LK or unfractionated bone marrow cells from P14 *Flt3*^{ITD}/*NHD13* mice, treated the cells briefly with Tat-Cre to delete the PGK-neo, and then performed limit dilution assays (Figure 5F-G).[36] The CD317^{+}LK fraction was highly enriched for engrafting cells (Figure 5H), and 12 of 14 engrafted recipients died of AML. These data confirm that the transcriptionally unique, IFN-1 responsive cell population in *NHD13* and *Flt3*^{ITD}/*NHD13* mice can initiate AML. They also raise the question of whether further cooperative changes in gene expression might be observed if CITE-seq assays were performed with *Flt3*^{ITDΔ} (ie, after removal of the PGK-neo cassette) rather than *Flt3*^{ITD}. Of note, the *Flt3*^{ITD}/*Runx1*^{DEL} mice described above carry *Vav1-Cre* and could be more appropriately described as *Flt3*^{ITDΔ}/*Runx1*^{DEL}. A summary of these alleles is provided in supplemental Table 5.

We repeated CITE-seq assays with P14 control, *Flt3*^{ITDΔ}, *NHD13,* and *Flt3*^{ITDΔ}/*NHD13* LK cells so that we could test whether enhanced FLT3^{ITD} signaling elicits additional cooperative changes in gene expression, and for further comparison with *Flt3*^{ITDΔ}/*Runx1*^{DEL}. We included B220 and CD317 as surface barcode markers and excluded B220 from the flow cytometry lineage cocktail. Both markers were more highly expressed in *Flt3*^{ITDΔ}/*NHD13* LK cells than in other genotypes by both flow cytometry and CITE-seq (supplemental Figure 7). The B220^{+} population may mark nascent AML cells (supplemental Figure 7A). We integrated single-cell transcriptomes from the original analysis for comparison purposes. *Flt3*^{ITDΔ}/*NHD13* dramatically reprogrammed hematopoiesis, yielding 2 prominent clusters, numbers 15 and 33, that expressed MPP3/4 surface markers but did not cluster near normal hematopoietic progenitors (Figure 5I; supplemental Figure 8A,E; supplemental Table 4). They accounted for a significantly greater percentage of LK cells in *Flt3*^{ITDΔ}/*NHD13* mice than was observed in single mutants or *Flt3*^{ITD}/*NHD13* (Figure 5J), thus demonstrating greater cooperation between the *Flt3*^{ITDΔ} and *NHD13* alleles than was observed with the weaker *Flt3*^{ITD} allele. Indeed, only 23% of the cells from the initial CITE-seq cluster 13 (Figure 4) mapped to cluster 33, and <0.2% mapped to cluster 15 (supplemental Figure 8B). *Runx1* deletion amplified *Flt3*^{ITDΔ}-driven expansion of MPP-like cluster 26 (supplemental Figure 8D-E). There was no overlap between clusters that emerged in *Flt3*^{ITDΔ}/*NHD13* and *Flt3*^{ITDΔ}/*Runx1*^{DEL} mice. Reactome pathway analysis redemonstrated enrichment for IFN-1 targets among cluster 33 marker genes and RAS pathway genes among cluster 15 markers (Figure 5K). Single-cell GSVA confirmed that IFN-1 target genes are significantly elevated in *Flt3*^{ITDΔ}/*NHD13* MPPs (based on CITE-seq tags) relative to *Flt3*^{ITDΔ}/*Runx1*^{DEL} and single-mutant MPPs, consistent with the prior analyses (Figure 5L).

We next tested whether genes that mark *Flt3*^{ITDΔ}/*NHD13* clusters are selectively expressed in *NUP98*-t mouse and human AML. We performed bulk RNA-seq on *Flt3*^{ITDΔ}/*NHD13* and previously collected *Flt3*^{ITDΔ}/*Runx1*$^{DEL/DEL}$ AML specimens[54] (deletion of both *Runx1* alleles was required for frank transformation). Principal component analysis revealed dramatic differences in gene expression between these genetically distinct leukemias (supplemental Figure 9A). GSVA showed that cluster 15 and 33 marker genes were enriched in *Flt3*^{ITDΔ}/*NHD13* AML, but not in *Flt3*^{ITDΔ}/*Runx1*$^{DEL/DEL}$ AML, as expected (Figure 5M). Importantly, cluster 33 (but not cluster 15) marker genes were highly expressed *NUP98*-translocated AML from 2 large pediatric AML RNA-seq data sets (TARGET and St. Jude),[1,40] relative to

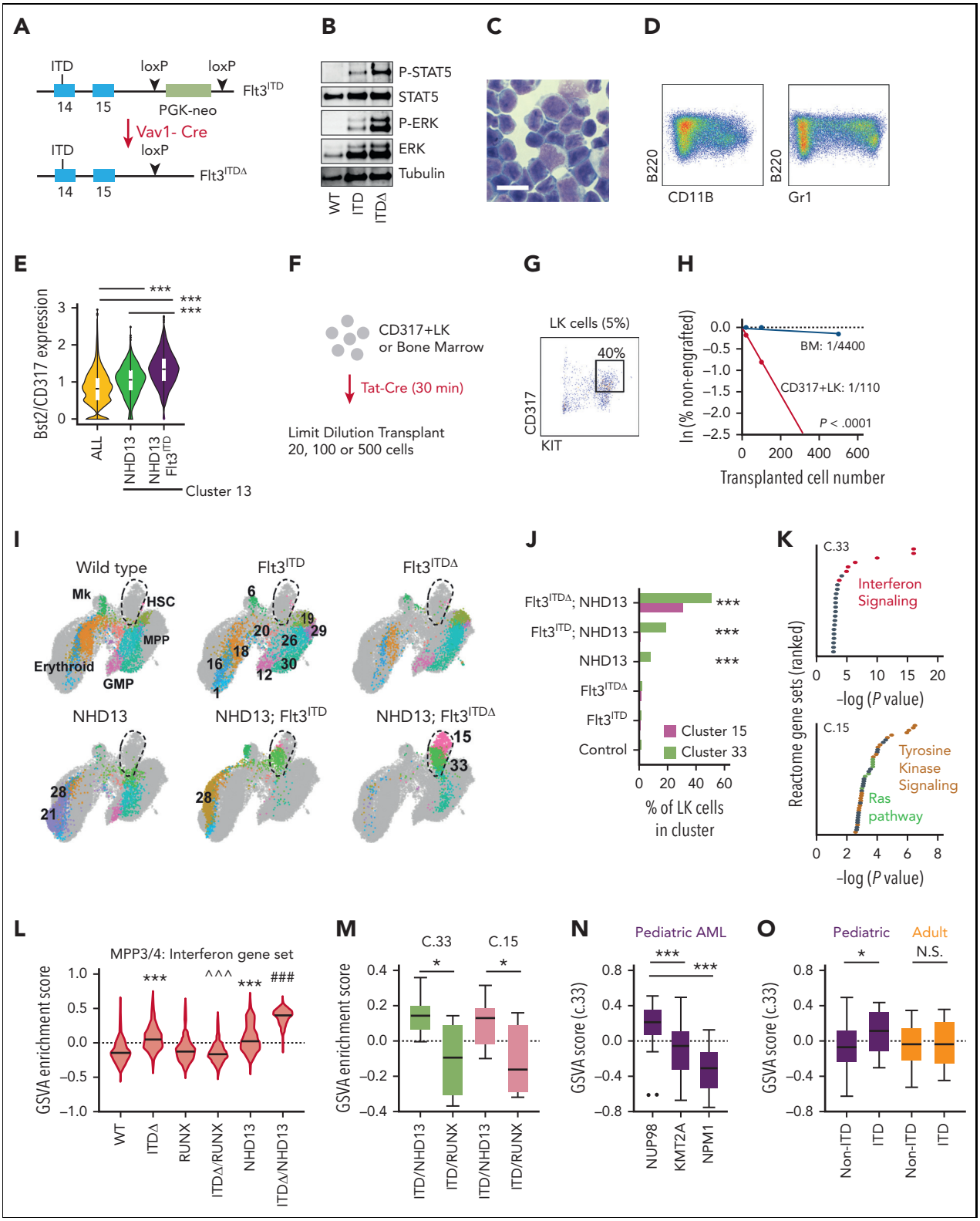

Figure 5. Enhanced FLT3^{ITD} signaling cooperates with *NHD13* to create an emergent, isolatable pre-AML population. (A) Diagram showing removal of PGK-neo cassette with *Vav1*-Cre. (B) Western blot showing elevated STAT5 and ERK phosphorylation in *Flt3*^{ITDΔ} MPPs. (C) Representative cytospin of *Flt3*^{ITDΔ}*/NHD13* AML. The scale bar indicates 20 μM. (D) Flow plot showing ectopic B220 expression in *Flt3*^{ITDΔ}*/NHD13* AML. (E) Normalized *Bst2*/CD317 expression in *NHD13* and *Flt3*^{ITDΔ}*/NHD13* LK cells based on CITE-seq experiments in Figure 4. The *NHD13* and *Flt3*^{ITDΔ}*/NHD13* columns reflect cells in cluster 13. "ALL" reflects cells in all other genotypes. ***$P < .0001$ based on the Wilcoxon rank sum test. (F) Overview of limiting dilution experiment after selection of CD317^{+}LK cells. (G) Flow cytometry plot showing CD317 expression in *Flt3*^{ITD}*/NHD13* LK cells. (H) Limiting dilution curves with comparison by extreme limiting dilution analysis.[36] (I) UMAP plots demonstrating clusters of cells from ICGS2 for the indicated genotypes. The heatmap is shown in supplemental Figure 8. *Runx1*^{DEL} clusters are also shown in supplemental Figure 8. (J) Bar graph showing percentages of cells for each genotype that populate clusters 15 and 33. Cluster 33 emerges with NHD13 and is amplified by *Flt3*^{ITD} and *Flt3*^{ITDΔ} (cluster 15 only emerges in *Flt3*^{ITDΔ}*/NHD13* mice).

KMT2A-rearranged and *NPM1*-mutated AML (Figure 5N; supplemental Figure 9B). The latter 2 mutations hyperactivate HOX genes, much like *NUP98*-t, and *NPM1* frequently cooperates with FLT3^{ITD} making these good benchmarks for comparison. Cluster 33 (but not cluster 15) marker genes were also highly expressed in pediatric but not adult *FLT3^{ITD}*-positive AML (The Cancer Genome Atlas) (Figure 5O; supplemental Figure 9C). Together, these observations show that *FLT3^{ITD}* and *NUP98*-t cooperate to elicit changes in gene expression and cell identity that are maintained in fully transformed AML and conserved in humans. Moreover, the changes are specific to pediatric *FLT3^{ITD}*-positive AML. *Flt3^{ITDΔ}/NHD13* mutations hyperactivate IFN-1 target genes, raising the question of whether IFN-1 promotes *NUP98*-t–AML initiation.

IFN-1 signaling promotes *Flt3^{ITD}/NHD13* AML initiation

We tested whether IFN-1 sustains *Flt3^{ITD}/NHD13* pre-AML cells by measuring HSC, MPP, pregranulocyte-monocyte progenitor (pGM), and GMP numbers (supplemental Figure 10A-B) in *Flt3^{ITD}/NHD13* mice, on either *Ifnar1$^{+/-}$* or *Ifnar1$^{-/-}$* backgrounds, at P0 or P14. *Ifnar1* encodes the IFN-1 receptor. *Ifnar1$^{+/-}$* served as a control, rather than *Ifnar1$^{+/+}$*, to simplify breeding strategies. We confirmed that *Ifnar1* heterozygosity had no perceivable effect on hematopoiesis in *Flt3^{ITD}/NHD13* mice (supplemental Figure 10C-G). *Ifnar1* deletion caused a near-complete loss of MPP2 and MPP3/4 subpopulations (CD150^{+}CD48^{+}Lineage^{-}Sca1^{+}Kit^{+} and CD150^{-}CD48^{+}Lineage^{-}Sca1^{+}Kit^{+}, respectively) at P14, particularly in mice with *NHD13* or *Flt3$^{ITD/+}$; NHD13* genotypes (Figure 6A-B). *Ifnar1* deletion also caused a concomitant expansion of phenotypic pGMs (Lineage^{-}Sca1^{-}Kit^{+}CD150^{-}CD105^{-}CD16/32^{-}) and GMPs (Lineage^{-}Sca1^{-}Kit^{+}CD150^{-}CD105^{-}CD16/32^{+}) in *Flt3^{ITD}/NHD13* mice (Figure 6C-D), without altering pGM or GMP proliferation or death rates (supplemental Figure 11A-D). Similar changes were observed at P0 (supplemental Figure 11E-H). *Ifnar1* deletion reduced the colony-forming activity of *Flt3^{ITD}/NHD13* MPP3/4s (Figure 6E), but competitive transplantation assays and limiting dilution transplants unexpectedly showed no difference in the repopulating activity of *Flt3$^{ITD/+}$; NHD13; Ifnar1$^{+/-}$* and *Flt3$^{ITD/+}$; NHD13; Ifnar1$^{-/-}$* bone marrow cells despite profound MPP depletion in the absence of *Ifnar1* (Figure 6F-G). Instead, phenotypic *Flt3^{ITD}/NHD13* pGMs repopulated recipient mice and offset the loss of MPPs (Figure 6H-J). These observations suggest that functional properties of hematopoietic progenitors, such as repopulating activity, may be decoupled from conventional surface marker phenotypes in *Flt3^{ITD}/NHD13* mice, especially after *Ifnar1* deletion (Figure 6K).

To reconcile this discrepancy, we performed additional CITE-seq experiments to clarify population-specific, IFN-1-dependent transcriptional changes using an approach that would not be confounded by changes in surface marker expression. We profiled control, *Flt3^{ITD}*, *NHD13,* and *Flt3^{ITD}/NHD13* progenitors, all on *Ifnar1$^{+/-}$* or *Ifnar1$^{-/-}$* backgrounds, clustered the cells with ICGS2 and overlaid established surface marker phenotypes for MPP and myeloid progenitor populations. As in Figure 4, we observed an emergent *NHD13*-dependent population (cluster #19 in this case) that expanded in the presence of *Flt3^{ITD}* (Figure 7A-B; supplemental Figure 12). The surface marker phenotypes of *NHD13* and *Flt3^{ITD}/NHD13* cells changed with *Ifnar1* deletion, shifting from a predominantly MPP2 phenotype to pGM/GMP phenotypes (Figure 7C-D). This likely explains why *Flt3$^{ITD/+}$; NHD13; Ifnar1$^{-/-}$* bone marrow cells retained repopulating activity despite near-complete loss of MPPs; the pGM/GMP-like cells were transcriptionally similar to *Flt3$^{ITD/+}$; NHD13; Ifnar1$^{+/-}$* MPPs, irrespective of their different surface marker phenotypes. *Ifnar1* deletion caused cluster 19 to contract in both *NHD13* and *Flt3^{ITD}/NHD13* mice (Figure 7B). It reduced the expression of the direct NUP98-NSD1 target *Cdk6*;[55] as well as self-renewal genes such as *Gata2* and *Msi2*, and inflammatory genes such as *Trim30a* and *Irf7* (Figure 7E; supplemental Table 6). Thus, IFN-1 modulates the size of an emergent pre-AML population in *NHD13* and *Flt3^{ITD}/NHD13* mice, and it enhances the expression of potential effectors of AML initiation.

We next tested whether IFN-1 signaling promotes *Flt3^{ITD}/NHD13*-driven AML. We generated *Flt3^{ITDΔ}; NHD13; Ifnar1$^{+/-}$* and *Flt3^{ITDΔ}; NHD13; Ifnar1$^{-/-}$* mice and compared their survival. *Flt3^{ITDΔ}; NHD13; Ifnar1$^{-/-}$* mice survived significantly longer than *Flt3^{ITDΔ}; NHD13; Ifnar1$^{+/-}$* mice (Figure 7F). We next took an orthogonal strategy that allowed us to activate *Flt3^{ITD}* after *NHD13*, rather than in parallel, to better mimic the sequential acquisition of mutations that occurs in humans. We isolated P0 LK cells from *NHD13; Ifnar1$^{+/-}$* and *NHD13; Ifnar1$^{-/-}$* mice and transduced them with MSCV-FLT3^{ITD}-IRES-mCherry retrovirus (Figure 7G). We transplanted the transduced cells into irradiated recipient mice and monitored survival. We observed similar engraftment efficiencies for each genotype (Figure 7H), but recipients of *NHD13; Ifnar1$^{-/-}$* cells survived significantly longer than recipients of *NHD13; Ifnar1$^{+/-}$* cells (Figure 7I). The mice died of acute megakaryoblastic leukemia (AMKL), irrespective of the *Ifnar1* genotype, based on CD41 expression within the mCherry-positive population (supplemental Figure 13A-B). STAT5 and ERK phosphorylation in the AMKL cells was comparable to levels in *Flt3^{ITDΔ}; NHD13* AML (supplemental Figure 13C). RNA-seq followed by GAGE pathway analysis showed that *Ifnar1*-deficient leukemias had

Figure 5 (continued) ***P < .0001 by χ^2 test relative to wild-type. Cluster 15 and 33 sizes were also significantly larger in *Flt3^{ITDΔ}/NHD13* relative to single mutants (P < .0001). (K) Reactome pathway analysis of cluster 33 and 15 marker genes. Significant gene ontology biological processes gene sets (FDR < 0.05) were ranked on the y-axis based on log(P values) shown on the x-axis. IFN-, tyrosine kinase- and RAS pathway-related gene sets are color coded as indicated. (L) GSVA scores for the IFN-1 target gene set in individual MPP3 or MPP4, based on surface barcode expression by CITE-seq. ***P < .001 relative to wild-type. ### IFN-1 signature enrichment is elevated relative to all other genotypes by one-way ANOVA and Holm-Sidak posthoc test, P < .001. ^^^IFN-1 signature enrichment is elevated relative to all other genotypes by one-way ANOVA and Holm-Sidak posthoc test, P < .001. (M) Cluster 15 and 33 markers were highly expressed in *Flt3^{ITDΔ}/NHD13* but not *Flt3^{ITDΔ}/Runx1$^{DEL/DEL}$* AML by GSVA. (N) GSVA analysis of cluster 33 markers in human *NUP98*-t AML relative to *KMT2A*-translocated or *NPM1*-mutated AML from combined TARGET and St. Jude pediatric data sets. (O) GSVA analysis of cluster 33 markers in human *FLT3^{ITD}*-positive or negative AML from TARGET (pediatric) and TCGA (adult) data sets. For panels M-O, *P < .05, ***P < .001 by Student t test. Box and whisker plots are shown by Tukey's method. ANOVA, analysis of variance; ERK, extracellular signal-regulated kinase; ICGS2, Iterative Clustering and Guide Gene Selection version 2; TCGA, The Cancer Genome Atlas.

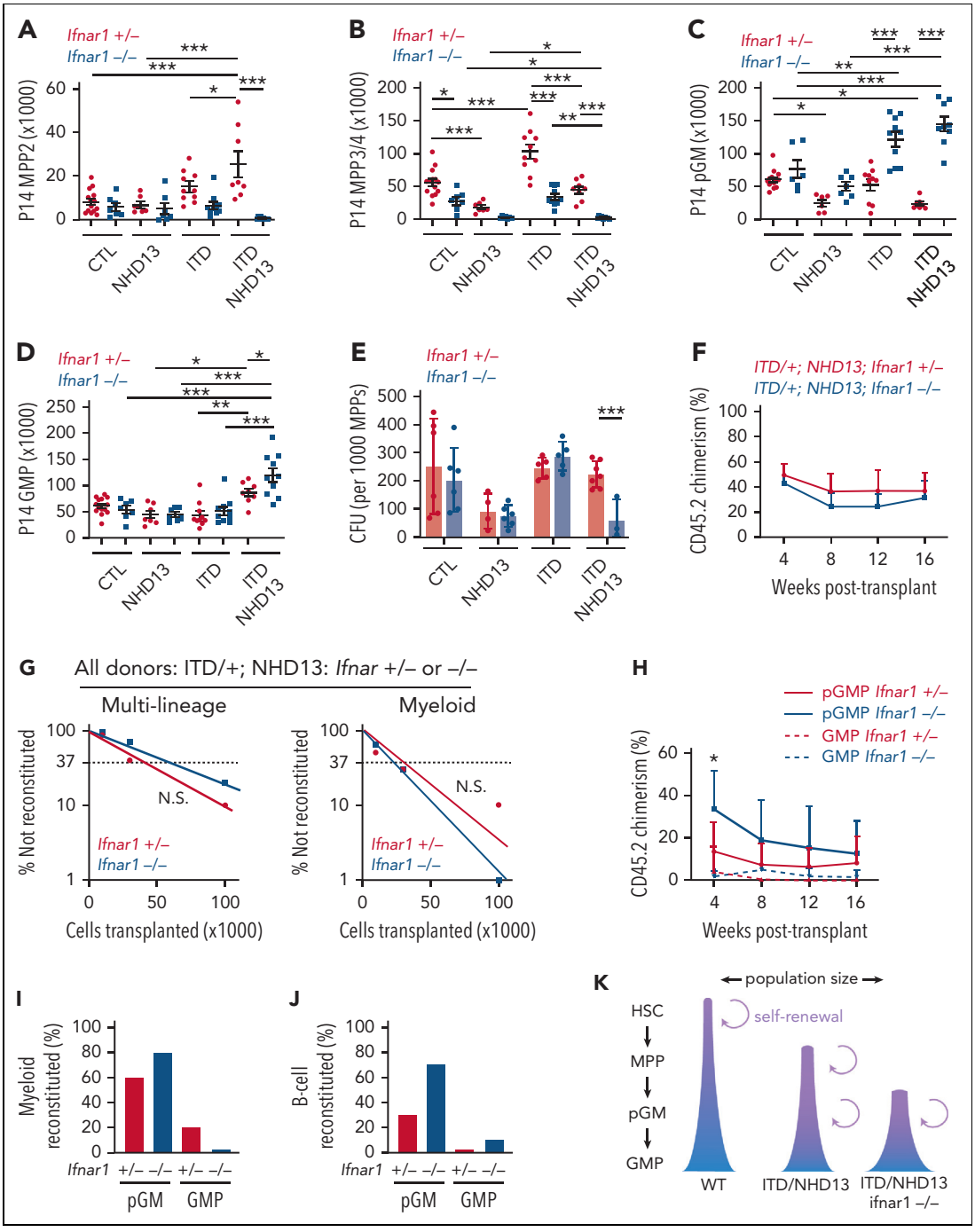

Figure 6. *Ifnar1* deletion in *NHD13* and *Flt3^{ITD}/NHD13* mice leads to phenotypic MPP depletion and myeloid progenitor expansion, without compromising repopulating activity. (A-D) MPP2, MPP3/4, pGM, and GMP numbers in P14 bone marrow for the indicated genotypes. n = 5 to 19. (E) CFUs per 1000 sorted MPP3/4s for the indicated genotypes. n = 3 to 7. (F) CD45.2 chimerism in recipients of 300 000 donor bone marrow cells of the indicated genotype competed with 300 000 CD45.1 wild-type bone marrow. n = 13 to 14. (G) Limiting dilution transplants from *Flt3^{ITD}/NHD13* bone marrow (on *Ifnar1$^{+/–}$* and *Ifnar1$^{–/–}$* backgrounds). Multilineage and myeloid engraftment results (reconstitution >1%) are shown. n = 10 to 14 per genotype per dose. There was no significant difference in repopulating activity by extreme limiting dilution analysis. (H) CD45.2 chimerism in recipients of 200 pGM or GMP of the indicated genotype competed with 300 000 CD45.1 wild-type bone marrow. n = 13 to 14. (I-J) Percent of recipients with myeloid or B-cell reconstitution after pGM and GMP transplants. (K) Conventional surface marker phenotypes do not reflect self-renewal capacity or lineage potential in *Flt3^{ITD}/NHD13* mice, particularly after *Ifnar1* deletion. Phenotypic MPPs and pGMs can self-renew, instead. For all panels, error bars reflect the standard deviation. *P < .05, **P < .01, ***P < .001 by one-way ANOVA with Holm-Sidak posthoc test. ANOVA, analysis of variance.

the reduced expression of genes associated with cell cycle progression and RNA processing/splicing (supplemental Figure 13D; supplemental Table 7). IFN-1, therefore, promotes AML/AMKL initiation.

The bulk RNA-seq and CITE-seq studies all predict that IFN-1 dependence should be specific to *Flt3^{ITD}/NHD13* AML initiation and not observed in *Flt3^{ITD}/Runx1^{DEL}* AML. The *Ifnar1* and *Runx1* alleles are closely linked on mouse

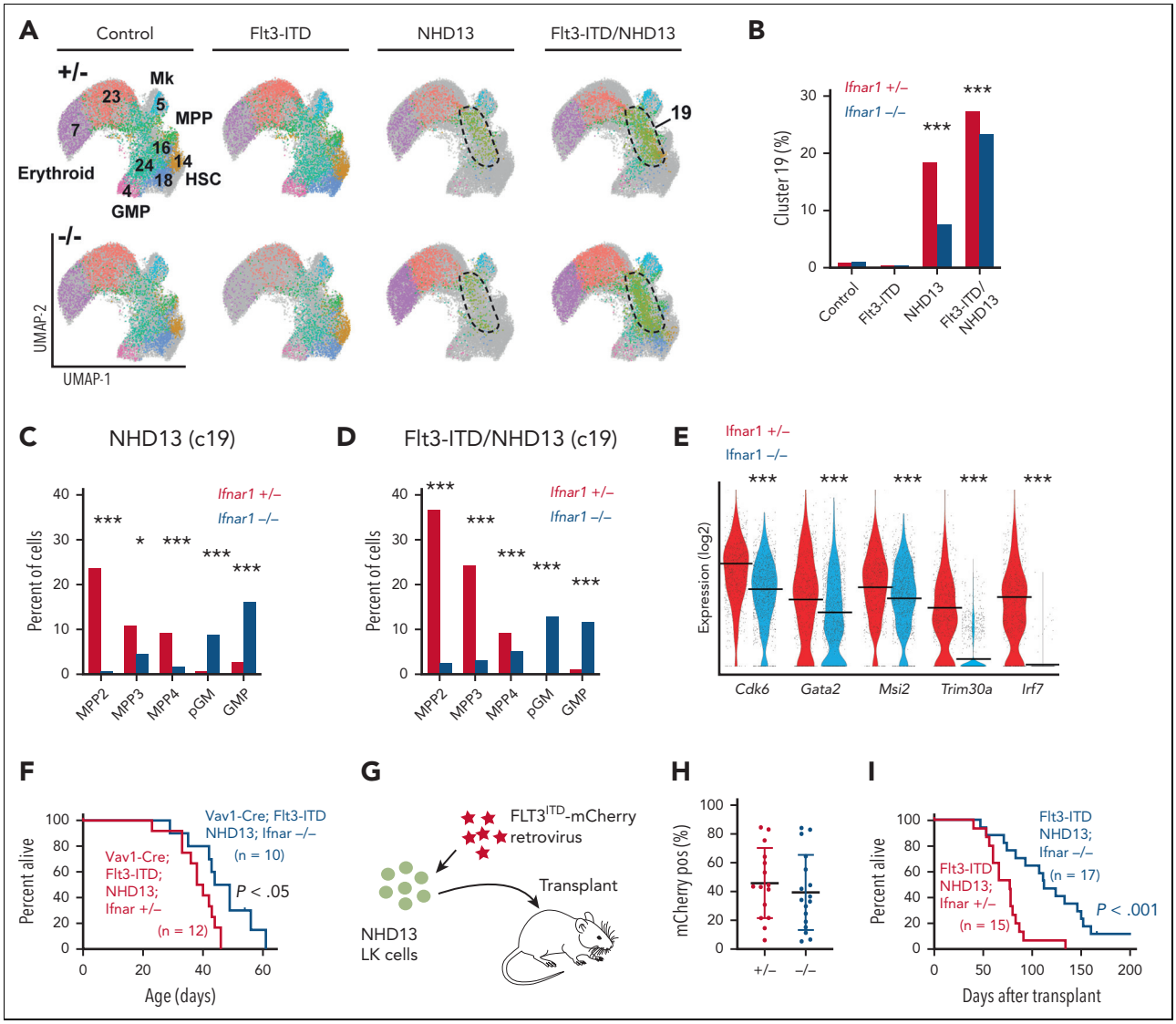

Figure 7. IFN-1 signaling potentiates *Flt3^{ITD}/NHD13* AML. (A) UMAP plots demonstrating clusters from ICGS2 for the indicated genotypes. In this case, cluster 19 demarcates an *NHD13*- and *Flt3^{ITD}/NHD13*-specific cluster based on marker genes (supplemental Table 6). The heatmap is shown in supplemental Figure 12. (B) Bar graph showing percentages of cells for each genotype that populate clusters 19. *Ifnar1* deletion depletes cluster 19 cells in *NHD13* and *Flt3^{ITD}/NHD13* mice. ***P < .0001 for *Ifnar1$^{+/-}$* vs *Ifnar1$^{-/-}$* by χ^2 test. (C-D) Surface marker phenotypes within cluster 19 are *Ifnar1*-dependent. In the absence of *Ifnar1*, cells lose MPP phenotypes and acquire pGM and GMP phenotypes despite very similar gene expression profiles. This is evident in both *NHD13* and *Flt3^{ITD}/NHD13* mice, indicating that conventional cell phenotypes do not adequately describe the transcriptional identities of cells that carry these mutations. *P < .05, ***P < .0001 for *Flt3^{ITD}/NHD13/Ifnar1$^{+/-}$* vs *Flt3^{ITD}/NHD13/Ifnar1$^{-/-}$* by χ^2 test. (E) Violin plots showing expression of several genes that are differentially expressed between *Flt3^{ITD}/NHD13/Ifnar1$^{+/-}$* and *Flt3^{ITD}/NHD13/Ifnar1$^{-/-}$* cluster 19 cells. ***P < .001 by Wilcoxon Rank Sum test. (F) Survival curves for *Vav1-Cre; Flt3^{ITD}; NHD13; Ifnar1$^{+/-}$* and *Vav1-Cre; Flt3^{ITD}; NHD13; Ifnar1$^{-/-}$* mice. (G) Schematic overview of survival experiments for an adoptive transfer model. LK cells were isolated from *NHD13* mice on *Ifnar1$^{+/-}$* or *Ifnar1$^{-/-}$* backgrounds and transduced with *Flt3^{ITD}*-expressing retrovirus. The cells were transplanted, and recipient survival was monitored. (H) mCherry chimerism for the indicated *Ifnar1* genotypes at 4 weeks after transplantation. (I) Survival curves for recipient mice that were transplanted with cells of the indicated genotypes. For panels F and I, survival curves were compared by the log-rank test. Group sizes are indicated in the panels. Adoptive transfer data reflect 4 independent experiments. ICGS2, Iterative Clustering and Guide Gene Selection version 2.

chromosome 16, making it impractical to test this hypothesis through conventional breeding strategies. Instead, we isolated HSCs/MPPs from *Flt3^{ITDΔ}; Ifnar1$^{+/-}$* and *Flt3^{ITDΔ}; Ifnar1$^{-/-}$* mice at P14 and inactivated *Runx1* by electroporating cells with a *Runx1*-specific–gRNA/Cas9 complex (supplemental Figure 14A). The cells were subsequently transplanted into lethally irradiated recipient mice. Editing efficiencies of >70% were confirmed by next-generation sequencing. Recipients began dying of AML at ~2 months after the transplant (supplemental Figure 14B-D). *Ifnar1* deletion did not affect survival. Thus, *Flt3^{ITD}/NHD13* cooperation conveys sensitivity to IFN-1 inactivation that is not observed with *Flt3^{ITD}/Runx1^{DEL}* cooperation.

Discussion

Our findings add a layer of complexity to established paradigms for oncogenic cooperation during AML initiation. Prior work has shown that *Flt3^{ITD}* elicits cooperative changes in gene expression and enhancer activation when paired with *Npm1*, *Tet2*, or *Runx1* mutations,[10,11,13] and the cooperative target gene profiles for these mutations overlap.[10] Activating *Nras*

mutations (eg, *Nras*^{G12D}) demonstrate similar patterns of cooperation with either *Tet2* or *Ezh2* mutations.[51,56] However, whereas prior studies examined interactions involving mutations that occur most commonly in adult AML, our current study suggests that interactions involving pediatric AML fusion proteins may be fundamentally different. Cooperative *Flt3*^{ITD}/*NHD13* target genes barely overlap with cooperative *Flt3*^{ITD}/*Runx1*^{DEL} target genes (Figure 2). Furthermore, *Flt3*^{ITD}/*NHD13* cooperation creates an emergent progenitor population that does not resemble normal hematopoietic progenitors or *Flt3*^{ITD}-mutant MPPs despite the expression of MPP surface markers (Figures 4 and 5). This emergent population can give rise to AML (Figure 5H), and cluster-specific marker genes are conserved in human pediatric *NUP98*-t AML (Figure 5M-N). The data show that *Flt3*^{ITD} coopts different mechanisms of transformation when it pairs with a pediatric-biased *NUP98*-t than with other, adult-biased AML mutations. These differences may ultimately create age- and cooperating mutation-specific vulnerabilities.

Our data reveal a context-specific role for IFN-1 signaling in AML initiation. We have shown that IFN-1 modulates the size of the emergent *NHD13*-dependent population of preleukemic progenitors, promotes the expression of self-renewal genes within that population, and potentiates leukemogenesis. Additional studies will be needed to test whether IFN-1 dependence extends to other cooperative interactions, such as those involving *Nras*^{G12D} or other NUP98 fusions. IFN-1 signaling is clinically actionable via IFNAR1/2 blocking antibodies or inhibitors of downstream signal transduction proteins (eg, the TYK2 inhibitor deucravacitinib).[57,58] Further studies will help identify patients who are most likely to benefit from IFN-1–directed therapies.

Acknowledgments

This work was supported by grants to J.A.M. from the National Institutes of Health (NIH), National Heart, Lung, and Blood Institute (R01 HL152180 and R01 HL136504) and the NIH, National Cancer Institute (NCI) (U01 CA267031), Alex's Lemonade Stand Foundation ("A" Award), Hyundai Hope On Wheels, the Alvin J. Siteman Cancer Center Investment Program (supported by the Foundation for Barnes-Jewish Hospital and NIH, NCI Cancer Center Support Grant P30 CA091842), the Leukemia and Lymphoma Society, and the Children's Discovery Institute of Washington University and St. Louis Children's Hospital. J.A.M. is a Leukemia and Lymphoma Society Scholar.

Authorship

Contribution: J.A.M. designed and oversaw all experiments and secured the funding; J.A.M. and Y.L. conducted experiments, interpreted data and wrote the manuscript; W.Y. performed all bioinformatic analyses; R.M.P., E.B.C., E.D., P.R.-L., and J.M.-C. performed experiments and interpreted data; and all authors reviewed and edited the manuscript.

Conflict-of-interest disclosure: The authors declare no competing financial interests.

ORCID profiles: Y.L., 0000-0003-4396-0557; R.M.P., 0000-0002-0169-1224; J.M.-C., 0000-0001-9558-152X; J.A.M., 0000-0002-0766-4200.

Correspondence: Jeffrey A. Magee, Washington University School of Medicine, 660 S. Euclid Ave, Box 8208, St. Louis, MO 63110; email: mageej@wustl.edu.

Footnotes

Submitted 2 May 2022; accepted 15 November 2022; prepublished online on *Blood* First Edition 17 November 2022. https://doi.org/10.1182/blood.2022016889.

Data sets generated are available at Gene Expression Omnibus under the SuperSeries accession GSE200559.

Data are available on request from the corresponding author, Jeffrey A. Magee (mageej@wustl.edu).

The online version of this article contains a data supplement.

There is a *Blood* Commentary on this article in this issue.

The publication costs of this article were defrayed in part by page charge payment. Therefore, and solely to indicate this fact, this article is hereby marked "advertisement" in accordance with 18 USC section 1734.

REFERENCES

1. Bolouri H, Farrar JE, Triche T Jr, et al. The molecular landscape of pediatric acute myeloid leukemia reveals recurrent structural alterations and age-specific mutational interactions. *Nat Med*. 2018;24(1):103-112.
2. Cancer Genome Atlas Research Network. Genomic and epigenomic landscapes of adult de novo acute myeloid leukemia. *N Engl J Med*. 2013;368(22):2059-2074.
3. Jan M, Snyder TM, Corces-Zimmerman MR, et al. Clonal evolution of preleukemic hematopoietic stem cells precedes human acute myeloid leukemia. *Sci Transl Med*. 2012;4(149):149ra118.
4. Lee BH, Williams IR, Anastasiadou E, et al. FLT3 internal tandem duplication mutations induce myeloproliferative or lymphoid disease in a transgenic mouse model. *Oncogene*. 2005;24(53):7882-7892.
5. Mallardo M, Caronno A, Pruneri G, et al. NPMc+ and FLT3_ITD mutations cooperate in inducing acute leukaemia in a novel mouse model. *Leukemia*. 2013;27(11):2248-2251.
6. Yang L, Rodriguez B, Mayle A, et al. DNMT3A loss drives enhancer hypomethylation in FLT3-ITD-associated leukemias. *Cancer Cell*. 2016;29(6):922-934.
7. Meyer SE, Qin T, Muench DE, et al. DNMT3A haploinsufficiency transforms FLT3ITD myeloproliferative disease into a rapid, spontaneous, and fully penetrant acute myeloid leukemia. *Cancer Discov*. 2016;6(5):501-515.
8. Rau R, Magoon D, Greenblatt S, et al. NPMc+ cooperates with Flt3/ITD mutations to cause acute leukemia recapitulating human disease. *Exp Hematol*. 2014;42(2):101-113.e105.
9. Mead AJ, Kharazi S, Atkinson D, et al. FLT3-ITDs instruct a myeloid differentiation and transformation bias in lymphomyeloid multipotent progenitors. *Cell Rep*. 2013;3(6):1766-1776.
10. Porter SN, Cluster AS, Yang W, et al. Fetal and neonatal hematopoietic progenitors are functionally and transcriptionally resistant to Flt3-ITD mutations. *Elife*. 2016;5:e18882.
11. Shih AH, Jiang Y, Meydan C, et al. Mutational cooperativity linked to combinatorial epigenetic gain of function in acute myeloid leukemia. *Cancer Cell*. 2015;27(4):502-515.
12. Greenblatt S, Li L, Slape C, et al. Knock-in of a FLT3/ITD mutation cooperates with a NUP98-HOXD13 fusion to generate acute myeloid leukemia in a mouse model. *Blood*. 2012;119(12):2883-2894.
13. Yun H, Narayan N, Vohra S, et al. Mutational synergy during leukemia induction remodels chromatin accessibility, histone modifications and three-dimensional DNA topology to alter gene expression. *Nat Genet*. 2021;53(10):1443-1455.
14. Michmerhuizen NL, Klco JM, Mullighan CG. Mechanistic insights and potential therapeutic approaches for NUP98-rearranged hematologic malignancies. *Blood*. 2020;136(20):2275-2289.

15. Ostronoff F, Othus M, Gerbing RB, et al. NUP98/NSD1 and FLT3/ITD coexpression is more prevalent in younger AML patients and leads to induction failure: a COG and SWOG report. *Blood*. 2014;124(15):2400-2407.

16. Hollink IH, van den Heuvel-Eibrink MM, Arentsen-Peters ST, et al. NUP98/NSD1 characterizes a novel poor prognostic group in acute myeloid leukemia with a distinct HOX gene expression pattern. *Blood*. 2011; 118(13):3645-3656.

17. Ahn JH, Davis ES, Daugird TA, et al. Phase separation drives aberrant chromatin looping and cancer development. *Nature*. 2021; 595(7868):591-595.

18. Chandra B, Michmerhuizen NL, Shirnekhi HK, et al. Phase separation mediates NUP98 fusion oncoprotein leukemic transformation. *Cancer Discov*. 2022;12(4):1152-1169.

19. Sun Y, Zhou B, Mao F, et al. HOXA9 reprograms the enhancer landscape to promote leukemogenesis. *Cancer Cell*. 2018; 34(4):643-658.e645.

20. Wang GG, Cai L, Pasillas MP, Kamps MP. NUP98-NSD1 links H3K36 methylation to Hox-A gene activation and leukaemogenesis. *Nat Cell Biol*. 2007;9(7):804-812.

21. Xu H, Valerio DG, Eisold ME, et al. NUP98 fusion proteins interact with the NSL and MLL1 complexes to drive leukemogenesis. *Cancer Cell*. 2016;30(6):863-878.

22. Thanasopoulou A, Tzankov A, Schwaller J. Potent co-operation between the NUP98-NSD1 fusion and the FLT3-ITD mutation in acute myeloid leukemia induction. *Haematologica*. 2014;99(9):1465-1471.

23. Struski S, Lagarde S, Bories P, et al. NUP98 is rearranged in 3.8% of pediatric AML forming a clinical and molecular homogenous group with a poor prognosis. *Leukemia*. 2017;31(3): 565-572.

24. Slape C, Liu LY, Beachy S, Aplan PD. Leukemic transformation in mice expressing a NUP98-HOXD13 transgene is accompanied by spontaneous mutations in Nras, Kras, and Cbl. *Blood*. 2008;112(5):2017-2019.

25. Mohanty S, Jyotsana N, Sharma A, et al. Targeted inhibition of the NUP98-NSD1 fusion oncogene in acute myeloid leukemia. *Cancers (Basel)*. 2020;12(10):2766.

26. Prigge JR, Hoyt TR, Dobrinen E, Capecchi MR, Schmidt EE, Meissner N. Type I IFNs act upon hematopoietic progenitors to protect and maintain hematopoiesis during pneumocystis lung infection in mice. *J Immunol*. 2015;195(11):5347-5357.

27. Lee BH, Tothova Z, Levine RL, et al. FLT3 mutations confer enhanced proliferation and survival properties to multipotent progenitors in a murine model of chronic myelomonocytic leukemia. *Cancer Cell*. 2007;12(4):367-380.

28. Taniuchi I, Osato M, Egawa T, et al. Differential requirements for Runx proteins in CD4 repression and epigenetic silencing during T lymphocyte development. *Cell*. 2002;111(5):621-633.

29. Lin YW, Slape C, Zhang Z, Aplan PD. NUP98-HOXD13 transgenic mice develop a highly penetrant, severe myelodysplastic syndrome that progresses to acute leukemia. *Blood*. 2005;106(1):287-295.

30. Li Y, Kong W, Yang W, et al. Single-cell analysis of neonatal HSC ontogeny reveals gradual and uncoordinated transcriptional reprogramming that begins before birth. *Cell Stem Cell*. 2020;27(5):732-747.

31. Chen R, Okeyo-Owuor T, Patel RM, et al. Kmt2c mutations enhance HSC self-renewal capacity and convey a selective advantage after chemotherapy. *Cell Rep*. 2021;34(7): 108751.

32. Porter SN, Cluster AS, Signer RA, et al. Pten cell autonomously modulates the hematopoietic stem cell response to inflammatory cytokines. *Stem Cell Reports*. 2016;6(6):806-814.

33. Gundry MC, Brunetti L, Lin A, et al. Highly efficient genome editing of murine and human hematopoietic progenitor cells by CRISPR/Cas9. *Cell Rep*. 2016;17(5): 1453-1461.

34. Pietras EM, Reynaud D, Kang YA, et al. Functionally distinct subsets of lineage-biased multipotent progenitors control blood production in normal and regenerative conditions. *Cell Stem Cell*. 2015;17(1):35-46.

35. Pronk CJ, Rossi DJ, Mansson R, et al. Elucidation of the phenotypic, functional, and molecular topography of a myeloerythroid progenitor cell hierarchy. *Cell Stem Cell*. 2007;1(4):428-442.

36. Hu Y, Smyth GK. ELDA: extreme limiting dilution analysis for comparing depleted and enriched populations in stem cell and other assays. *J Immunol Methods*. 2009;347(1-2): 70-78.

37. Butler A, Hoffman P, Smibert P, Papalexi E, Satija R. Integrating single-cell transcriptomic data across different conditions, technologies, and species. *Nat Biotechnol*. 2018;36(5):411-420.

38. Venkatasubramanian M, Chetal K, Schnell DJ, Atluri G, Salomonis N. Resolving single-cell heterogeneity from hundreds of thousands of cells through sequential hybrid clustering and NMF. *Bioinformatics*. 2020; 36(12):3773-3780.

39. Hanzelmann S, Castelo R, Guinney J. GSVA: gene set variation analysis for microarray and RNA-seq data. *BMC Bioinformatics*. 2013;14:7.

40. McLeod C, Gout AM, Zhou X, et al. St. Jude Cloud: a pediatric cancer genomic data-sharing ecosystem. *Cancer Discov*. 2021; 11(5):1082-1099.

41. Dobin A, Davis CA, Schlesinger F, et al. STAR: ultrafast universal RNA-seq aligner. *Bioinformatics*. 2013;29(1):15-21.

42. Ritchie ME, Phipson B, Wu D, et al. limma powers differential expression analyses for RNA-sequencing and microarray studies. *Nucleic Acids Res*. 2015;43(7):e47.

43. Joshi-Tope G, Gillespie M, Vastrik I, et al. Reactome: a knowledgebase of biological pathways. *Nucleic Acids Res*. 2005; 33(database issue):D428-D432.

44. Luo W, Friedman MS, Shedden K, Hankenson KD, Woolf PJ. GAGE: generally applicable gene set enrichment for pathway analysis. *BMC Bioinformatics*. 2009;10:161.

45. Subramanian A, Tamayo P, Mootha VK, et al. Gene set enrichment analysis: a knowledge-based approach for interpreting genome-wide expression profiles. *Proc Natl Acad Sci U S A*. 2005;102(43):15545-15550.

46. Corces MR, Trevino AE, Hamilton EG, et al. An improved ATAC-seq protocol reduces background and enables interrogation of frozen tissues. *Nat Methods*. 2017;14(10): 959-962.

47. Schmidl C, Rendeiro AF, Sheffield NC, Bock C. ChIPmentation: fast, robust, low-input ChIP-seq for histones and transcription factors. *Nat Methods*. 2015; 12(10):963-965.

48. Roadmap Epigenomics Consortium, Kundaje A, Meuleman W, et al. Integrative analysis of 111 reference human epigenomes. *Nature*. 2015;518(7539):317-330.

49. Li Q, Brown JB, Huang H, Bickel PJ. Measuring reproducibility of high-throughput experiments. *Ann Appl Stat*. 2011;5(3): 1752-1779.

50. Zhou X, Lowdon RF, Li D, et al. Exploring long-range genome interactions using the WashU Epigenome Browser. *Nat Methods*. 2013;10(5):375-376.

51. Liu Y, Gu Z, Cao H, et al. Convergence of oncogenic cooperation at single-cell and single-gene levels drives leukemic transformation. *Nat Commun*. 2021;12(1): 6323.

52. Cauchy P, James SR, Zacarias-Cabeza J, et al. Chronic FLT3-ITD signaling in acute myeloid leukemia is connected to a specific chromatin signature. *Cell Rep*. 2015;12(5): 821-836.

53. Olsson A, Venkatasubramanian M, Chaudhri VK, et al. Single-cell analysis of mixed-lineage states leading to a binary cell fate choice. *Nature*. 2016;537(7622): 698-702.

54. Porter SN, Magee JA. PRKCH regulates hematopoietic stem cell function and predicts poor prognosis in acute myeloid leukemia. *Exp Hematol*. 2017;53:43-47.

55. Schmoellerl J, Barbosa IAM, Eder T, et al. CDK6 is an essential direct target of NUP98 fusion proteins in acute myeloid leukemia. *Blood*. 2020;136(4):387-400.

56. Kunimoto H, Meydan C, Nazir A, et al. Cooperative epigenetic remodeling by TET2 loss and NRAS mutation drives myeloid transformation and MEK inhibitor

sensitivity. *Cancer Cell*. 2018;33(1):44-59.e48.

57. Gonciarz M, Pawlak-Bus K, Leszczynski P, Owczarek W. TYK2 as a therapeutic target in the treatment of autoimmune and inflammatory diseases. *Immunotherapy*. 2021;13(13):1135-1150.

58. Papp K, Gordon K, Thaci D, et al. Phase 2 Trial of selective tyrosine kinase 2 inhibition in psoriasis. *N Engl J Med*. 2018;379(14):1313-1321.